Electronic Supplementary Materials (ESI) for New Journal of chemistry

Supplementary information

Highly sensitive *in-situ* SERS monitoring of fenton-like reaction

by PDDA-MXene@AuNPs composite

Yun Bai, Tunmise Ayode Otitoju, Yun Wang, Qiong Chen, Ting Sun *

College of Sciences, Northeastern University, 3-11, Wenhua Road, Shenyang, Liaoning, 110819, China.

S1. Experimental Section

1. Chemicals and Reagents

Lithium fluoride, concentrated hydrochloric acid, $HAuCl_4$ (chlorauric acid), PDDA (polydiallyl dimethyl ammonium chloride) were purchased from Shanghai Maclin. Crystal violet and thiram were purchased from Aladdin reagent (Shanghai) Co. LTD. Biochemical Technology Co. LTD., Ti_3AlC_2 (aluminum carbon titanium) was purchased from Jilin 11 Technology Co. Ltd. All chemicals were used without further purification.

2. Apparatus and Instruments

The morphologies of the samples were observed using the scanning electron microscope (SEM, SU8000, Hitachi) equipped with an energy dispersive spectrometer system (EDS, EDAX-Ametek) and transmission electron microscopy (TEM, JEM-2000EX). FT-IR spectra were recorded using a KBr pellet in the range of 4000-500 cm^{-1} on a PerkinElmer Spectrum One (B) spectrometer to evaluate the functional groups. The X-ray diffraction (XRD) of samples was obtained using a Bruker D8 with Cu-Kα radiation (λ=1.54 A) at 40 kV and 40 mA. Atomic force microscopy (AFM) was conducted on the drop-cast flakes on a Si/SiO2 substrate using the Bruker Multimode 8 atomic force microscope in tapping mode in a glovebox. The zeta potentials were measured using micro-electrophoresis apparatus (ZEN1690, UK). The specific surface area was calculated according to the Brunauer-Emmett-Teller (BET) method and the pore size distribution was analyzed using the Density Functional Theory (DFT) method. X-ray photoelectron spectroscopy (XPS) was used to analyze the composition of materials (Thermo Instruments Inc, USA). UV–vis spectrophotometer (T6, Beijing Purkinje General Instrument Co., Ltd.) and Raman spectra (BWS465-785s) were used to monitor the Fenton-like process.

3. Synthesis of $Ti_3C_2T_x$ nanosheets

The $Ti_3C_2T_x$ nanosheets were prepared by etching Al atoms from Ti_3AlC_2 in a mixture of lithium fluoride and concentrated hydrochloric acid. Firstly, different molar ratios of etchants (HCl: LiF= 2, 2.5, 3) were mixed and then one gram of Ti_3AlC_2 powder was introduced into the solution for five minutes in batches under an ice bath. Thereafter, the solution was stirred at 40℃ for 48 hours. The solution was centrifuged at 10000 rpm and repeated until the pH reached about 7. The clay-like black precipitate was redispersed in 150 mL of deionized water and sonicated for 1 hour with nitrogen under an ice bath. The dispersion was centrifuged for 30 minutes at 3500 rpm, and the dark $Ti_3C_2T_x$ supernatants were obtained. Lastly, the colloidal solution was stored at 4℃.

4. Synthesis of PDDA- $Ti_3C_2T_x$ @AuNPs composite

1 ml PDDA was dropped slowly into 30 ml MXene solution and stirred at room temperature for 24 hours. The mixture was washed and centrifuged, and the precipitate was re-dispersed to obtain PDDA-$Ti_3C_2T_x$ solution. AuNPs were prepared according to a similar synthesis method.[1] Briefly, 339.8 ul of 58.85 M sodium citrate was added into boiling 1 mM $HAuCl_4$ solution (10 ml) until the solution turned purple-red. Subsequently, it was soaked in ice water to cool and centrifuged at 5000 rpm and the PH is around 5.5. The precipitate was re-dispersed to obtain AuNPs solution. The volume ratio of AuNPs solution and PDDA-$Ti_3C_2T_x$ solution was 1:5. Finally, the mixed solution was stirred for 2 hours to obtain PDDA-$Ti_3C_2T_x$ @AuNPs.

5. SERS performance of PDDA-$Ti_3C_2T_x$@AuNPs

PDDA-$Ti_3C_2T_x$@AuNPs were further used as SERS substrates for the detection of probe molecules, pure MXene and AuNPs were also used here to investigate the SERS mechanism. The SERS substrate was introduced in the target solutions of CV and thiram with the ratio (V/V%) of 1:1. After 1 hour, 50 ul of aliquot was extracted from the mixture and measured using the portable Raman spectrometer at a wavelength of 785 nm. The spectra were taken at a range of 200-2000 cm^{-1} with an acquisition time of 20 s.

6. The fenton-like reaction of PDDA-MXene@AuNPs investigated by UV-Vis

The catalytic performance of the material was investigated for CV by UV-Vis. Briefly, 10 mg of PDDA-MXene@AuNPs was mixed in 50 ml of 20 mg/l CV solution. After stirring for 30 minutes, 100 ul of H2O2(30%) was added to the mixture. Thereafter, 4 ml of aliquot was extracted at 5 mins intervals from the solution and measured using a UV-visible spectrophotometer. To investigate the mechanism, isopropanol was used as the quenching agent for hydroxyl radicals and the same amount of PDDA-MXene, AuNPs were used as catalyst.

7. In-situ SERS monitoring of Fenton-like reaction for PDDA-MXene@AuNPs

Simply, PDDA-Ti_3C_2Tx@AuNPs composite was mixed with $0.1225×10^{-6}$ M CV for 1 hour and put it into a 90 mm culture dish. For the SERS monitoring process, 785 nm laser with same parameter before was focused on the surface of the mixture and the SERS signal was recorded with 5 minutes intervals once the H_2O_2(30%) was added into the dish.

S2. Additional Figures
1. SEM, XRD of MXene by different etchants ratios and mapping of few-layered MXene
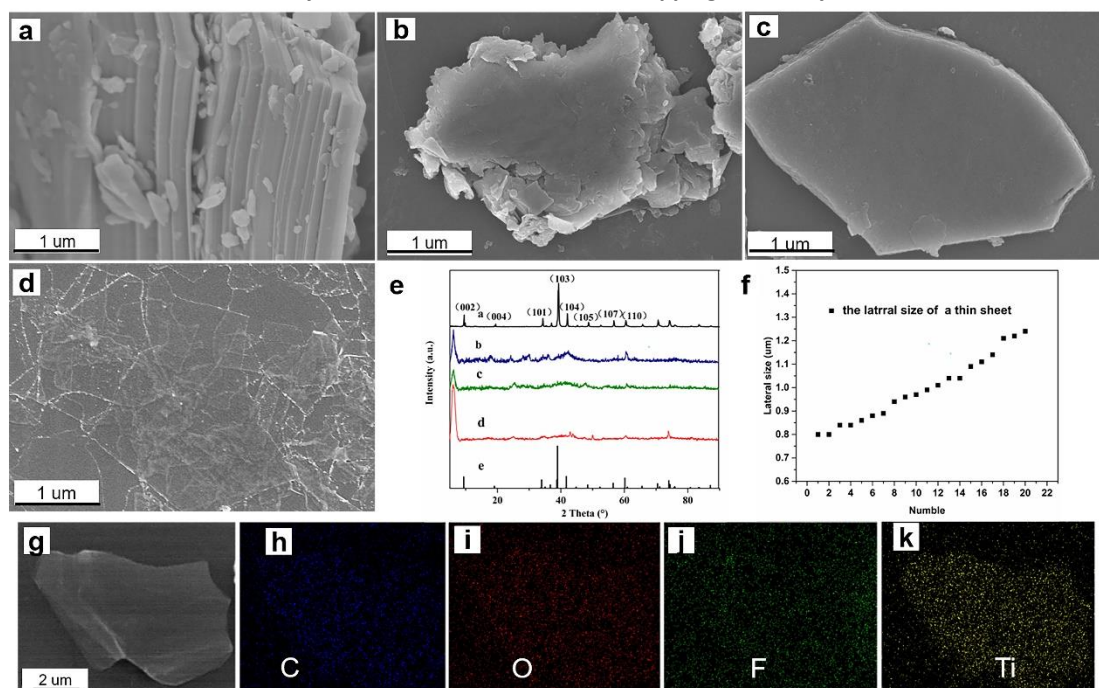

Fig. S1 Characterization of the MXene ($Ti_3C_2T_x$) nanosheets. (a) SEM image of precursor Ti_3AlC_2; (b) $Ti_3C_2T_x$-2 solutions (HCl: LiF= 2); (c) $Ti_3C_2T_x$-2.5 solutions (HCl: LiF= 2.5); (d) $Ti_3C_2T_x$-3 solutions (HCl: LiF= 3); (e) XRD of MXene; (f) Lateral size of a thin sheet in (d); (g-k) elemental mapping of few-layered MXene.

During the preparation of a few-layered MXene, many factors such as etching agent, temperature and time affect the etching result. Herein, we optimized the molar ratio of etchants. $Ti_3C_2T_x$ was etched at different molar ratios of etchants (HCl: LiF= 2, 2.5, 3), which called $Ti_3C_2T_x$-2, $Ti_3C_2T_x$-2.5, $Ti_3C_2T_x$-3. The XRD and SEM images are presented in Fig. S1. As seen in Figure S1(a-d), the layers become larger and thinner and the lateral size of a thin sheet in (d) is 0.8-1.2 um. The XRD of MXene in Figure S1(e) matches with the standard card pattern of the precursor Ti_3AlC_2 (00-052-0875). Fig. S1(e) shows the XRD of MXene solutions at different etchant ratios. As seen, the peak of (002) gradually becomes stronger and the peak of (104) gradually decreases with the increase in the molar ratio of etching agent. The disappearance of (104) peak at 39° for $Ti_3C_2T_x$-3 indicates the complete removal of Al atom in the precursor. [2] At the same time, the (002) peak widened and shifted to the left, signifying no existence of a metal bond between $Ti_3C_2T_x$ layers after the removal of Al element and introduction of surface terminal groups (-F, -O, -Oh). As a result, the distance between layers becomes wider. Figure S1(g)-(k) are the element mapping of few-layered MXene, which indicate the few-layered MXene was made of C, O, F and Ti elements. Therefore, the optimum molar ratio of the etchant is 3. Under this condition, few-layered $Ti_3C_2T_x$ nanosheets were successfully prepared. The reaction equation is as followed:

$$2Ti_3AlC_2 + 6LiF + 6HCl = 2Ti_3C_2 + Li_3AlF_6 + AlCl_3 + 3LiCl + 3H_2 \quad (1)$$
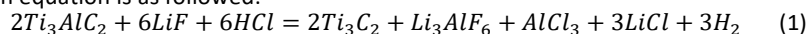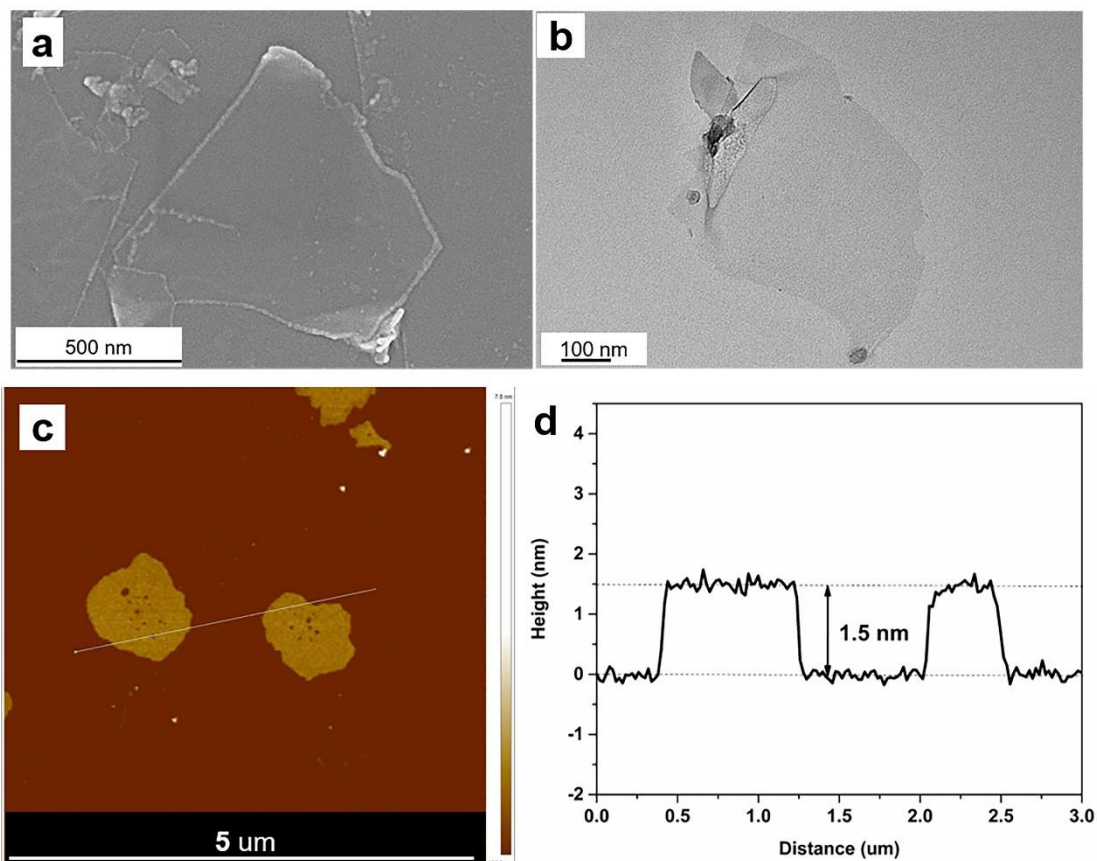
2. The morphology of Ti₃C₂Tₓ nanosheets

Fig.S2. The morphology of Ti$_3$C$_2$T$_x$ nanosheets. (a) SEM; (b) TEM; (c) AFM and (d) measured thickness of few-layered MXene.

3. The N₂ adsorption desorption isotherm of few-layered Ti₃C₂Tₓ
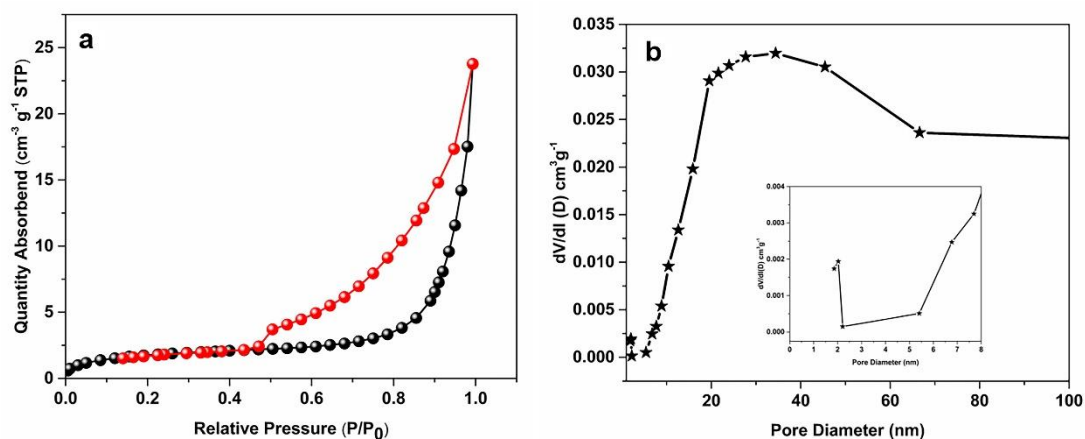

Fig.S3. (a) N$_2$ adsorption-desorption isotherm; (b) pore size distribution.

The pore distribution of Ti$_3$C$_2$T$_x$ nanosheets and N$_2$ adsorption-desorption isotherm is shown in Figure S3. The results show that all samples exhibit type V nitrogen adsorption isotherm with a distinct hysteresis loop at relative pressures (P/ P$_0$) ranging from 0.4 to 1 in Figure S3(a). As seen in Figure S3(b), the pore size of Ti$_3$C$_2$T$_x$ nanosheets ranges from 2 to 50 nm, indicating that the sample is made of mesoporous and microporous structures.
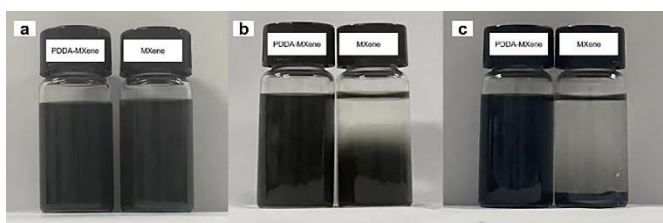
4. Images of MXene and PDDA-Mxene

Fig.S4. The Stability of complex in aqueous solution at 20℃ at a different time (a) t=0 h; (b) t=12 h; (c) t=24 h.

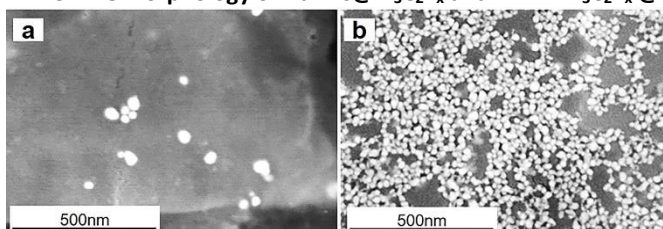## 5. The morphology of AuNPs@Ti$_3$C$_2$T$_x$ and PDDA-Ti$_3$C$_2$T$_x$ @AuNPs

Fig.S5. (a) SEM of Ti$_3$C$_2$T$_x$@AuNPs; (b) SEM of PDDA- Ti$_3$C$_2$T$_x$@AuNPs.

Observably SEM of Ti$_3$C$_2$T$_x$@AuNPs and PDDA- Ti$_3$C$_2$T$_x$@AuNPs, it can be seen that after the introduction of PDDA, a large number of dense AuNPs particles were successfully loaded on the Ti$_3$C$_2$T$_x$ nanosheets in Figure S5(b), which is conducive for the generation of a large number of "hot spots",[3] beneficial for the LSPR effect and thus enhance the SERS properties. For the sample without PDDA in Figure S5(a), the AuNPs were scattered and aggregated, which may decrease the LSPR effect.
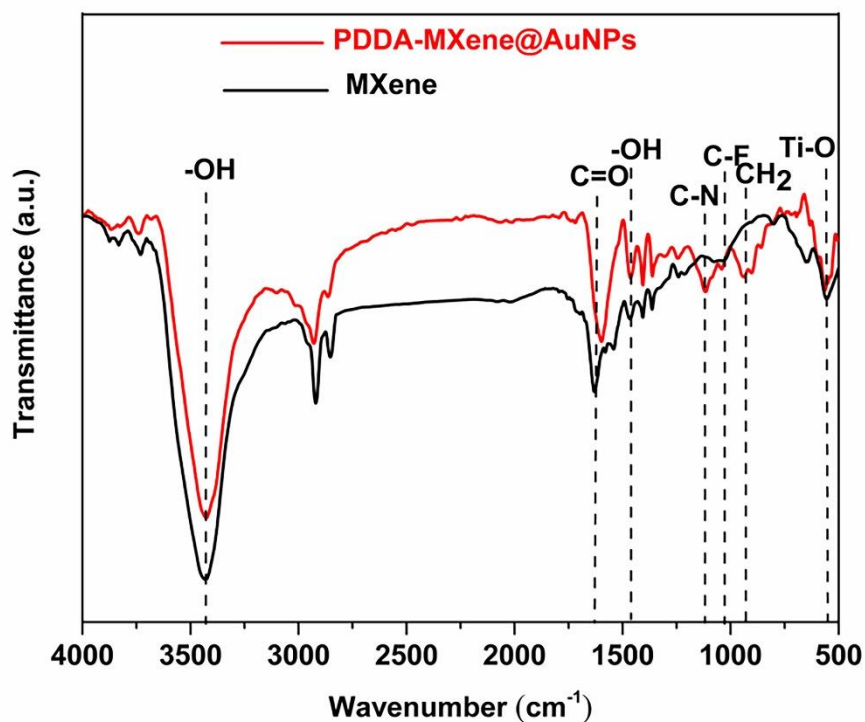
6. The FT-IR of PDDA-MXene@AuNPs

Fig.S6. FT-IR of MXene and PDDA-MXene@AuNPs.
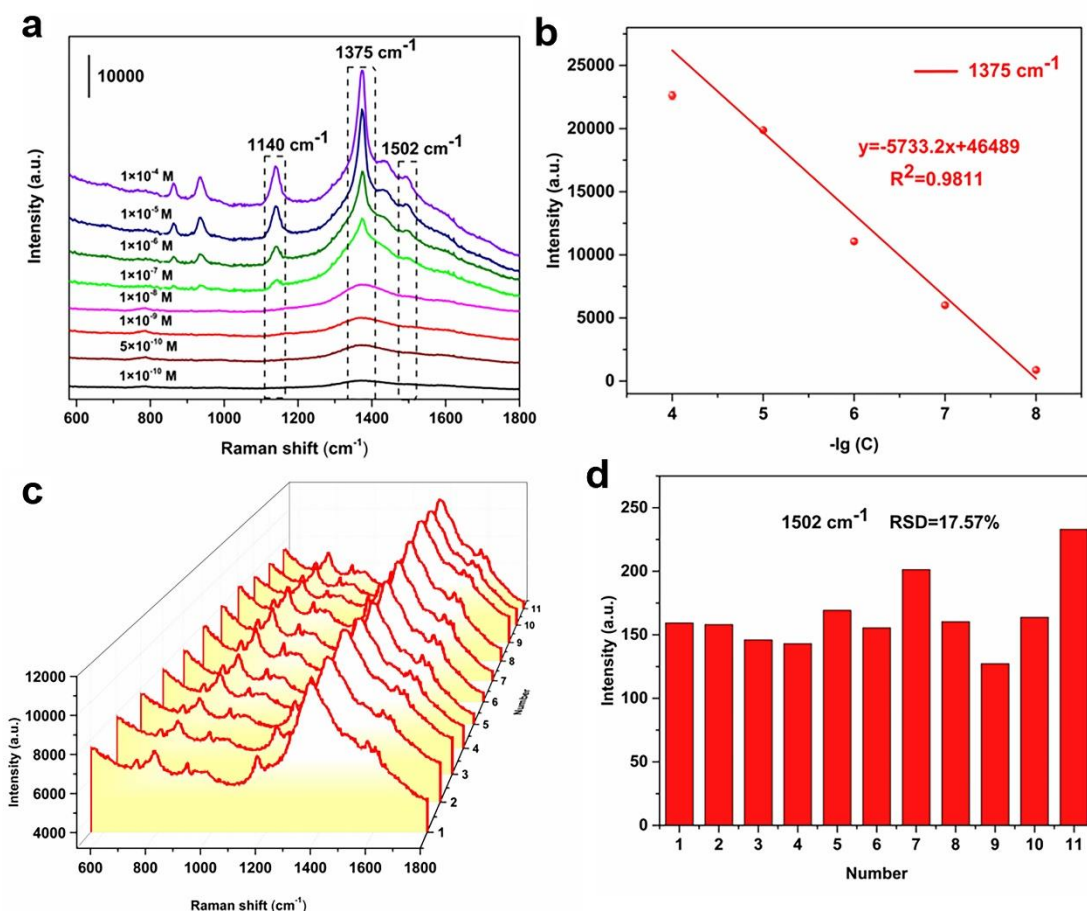
7. SERS spectra of thiram

Fig. S7. (a) SERS spectra of thiram at different concentration; (b) Intensity-concentration relationship based on the characteristic peaks at 1375 cm^{-1}; (c) eleven cycling runs of the PDDA-MXene@AuNPs composite for thiram (1×10^{-6} M); (d) the RSD at 1375 cm^{-1}.

8. The selectivity of the PDDA-Ti$_3$C$_2$T$_x$@AuNPs SERS substrate
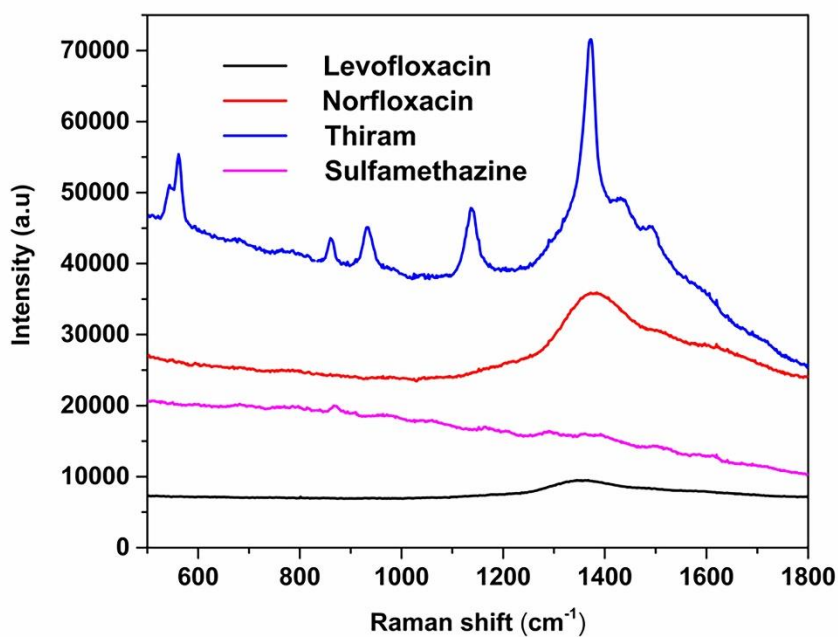

Fig. S8. Selectivity of the PDDA-Ti$_3$C$_2$T$_x$@AuNPs SERS substrate of levofloxacin, norfloxacin, thiram and sulfamethazine.

The PDDA-MXene@AuNPs composite was not effective for treating other organic pollutants with benzene ring structure, including levofloxacin, norfloxacin and sulfamethazine. As seen from the SERS spectra, only thiram could achieve SERS enhancement, which further confirms the selectivity of the PDDA-MXene@AuNPs composite.
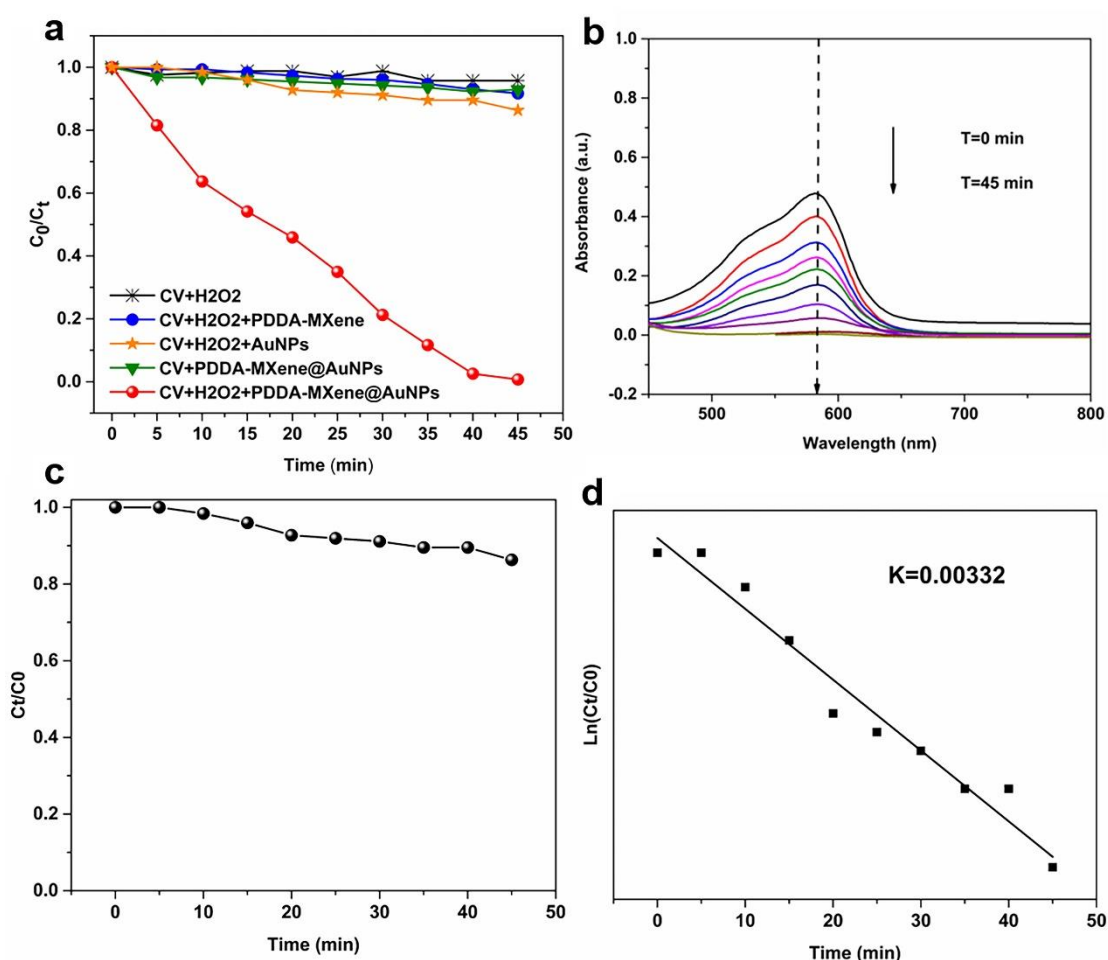
9. UV-Vis monitoring of CV degradation process

Fig. S9. (a) Fenton-like reaction of PDDA-Ti$_3$C$_2$T$_x$ @AuNPs monitored by UV-vis; (b) UV-vis spectra of the Fenton-like reaction; (c) and (d) Quenching reaction of hydroxyl radical of isopropanol.

The heterogeneous Fenton-like reaction was monitored by UV-vis in Figure S9. The concentration of CV during the reaction was given by the standard curve of CV in Figure S10 and the catalytic efficiency of PDDA-Ti$_3$C$_2$T$_x$@AuNPs was calculated as 99.32% after 45 mins, signifying an enhanced Fenton-like activity.

To verify the function of PDDA-Ti$_3$C$_2$T$_x$@AuNP, the same amount of CV was mixed with H$_2$O$_2$, and the results in Figure S9(a) show that the concentration almost remains the same throughout the reaction. In order to investigate the Fenton-like mechanism, the PDDA-MXene and AuNPs were used as cocatalysts. The result shows that the combination of CV+H$_2$O$_2$+PDDA-MXene did not show a significant effect on the degradation of CV, and only 8% degradation rate was achieved. This signifies that the PDDA-MXene@AuNPs exhibit excellent catalytic performance, which may be due to the addition of AuNPs. Meanwhile, the degradation rate of CV+H$_2$O$_2$+ AuNPs was only 13.71%. The result further confirms the conclusion that gold nanoparticles in the absence of a carrier are easy to agglomerate due to the van der Waals forces, which may reduce the surface area and restrict the catalytic activity. Therefore, the main reason for the excellent Fenton-like property of PDDA-MXene@AuNPs can be due to the synergistic effect of MXene and AuNPs. The degradation rate (%) was evaluated using the following equation [4]:

$$D = \frac{C_0 - C_t}{C_0} \qquad (2)$$

where D is the degradation rate, C$_0$ and C$_t$ are the concentration of CV at time (0) and time (T), respectively. The rate constant was determined according to the typical pseudo-first-order kinetic [5]:

$$\ln \frac{C_0}{C_t} = kt \qquad (3)$$

where C$_0$ and C$_t$ represent the initial concentration and the concentration at time T, k is the pseudo-first-order reduction rate constant. The k value of AuNPs, PDDA-MXene and PDDA-MXene@AuNPs are 0.0041 min^{-1}, 0.0023 min^{-1} and 0.09791 min^{-1}, separately. This proves that the reaction follows the pseudo-first-order kinetics. Figure S9(b) shows the UV-Vis spectra of CV's degradation using PDDA-

Ti$_3$C$_2$T$_x$@AuNPs. The maximum absorption peak of CV at 583 nm decreases gradually with the increase of reaction time until it nearly reaches zero.

The quenching experiment of hydroxyl radical in Figure S9 (c) and (d) was carried out with quencher isopropanol, which shows the effect of quenching agent on the degradation of CV, where the k value was 0.00332 min^{-1}, indicating that the major active specie is the generated OH.
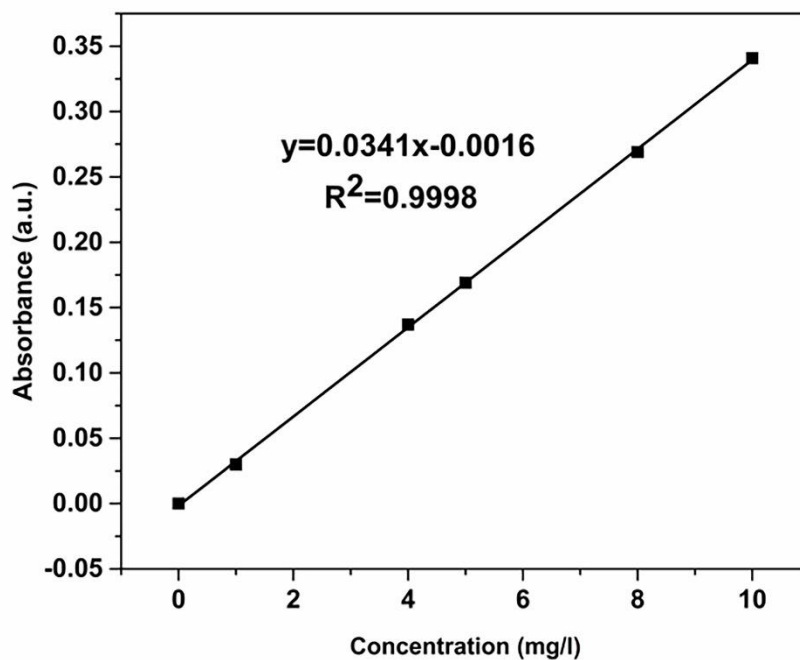
10. UV-vis standard curve of CV

Fig. S10. UV-vis standard curve of CV.

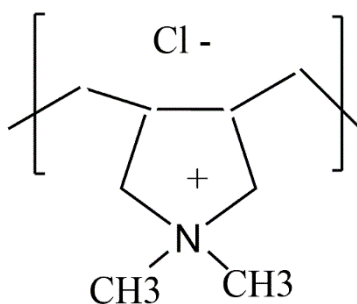### 11. Structure of PDDA，Crystal violet and Thiram

PDDA:

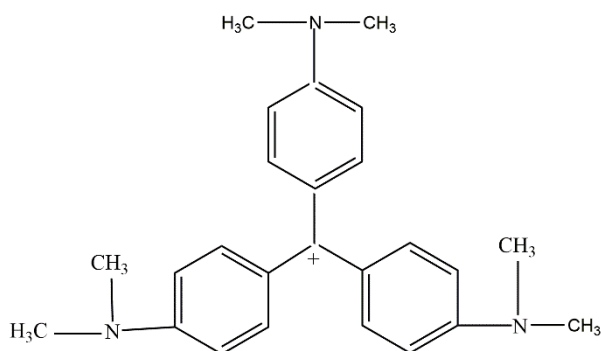**Fig. S11.** The structure of Poly dimethyl diallyl ammonium chloride (PDDA).

Crystal Violet：

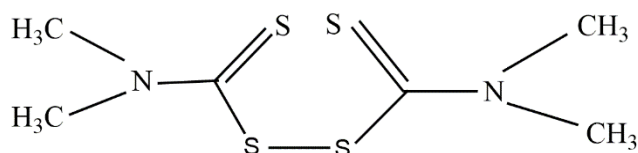**Fig. S12.** The structure of crystal violet (CV).

Thiram:

Fig. S13. The structure of thiram.

12. Zeta potential of MXene and PDDA-MXene

	$Ti_3C_2T_x$	PDDA-$Ti_3C_2T_x$
Zeta potential(mV)	-24.3	26.6

Table S1. Zeta potential of pristine $Ti_3C_2T_x$ and PDDA-Ti_3C_2T.

13. Table 2. The SERS detection limit of Crystal Violet compared by other's works

substrate	Probe molecule	Sensitivity	Ref.
MXene/Au	Crystal Violet	1×10^{-8} M	[6]
MoS2@TiO2@Au	Crystal Violet	1.23×10^{-6} M	[7]
Au@PBNPs	Crystal Violet	1×10^{-9} M	[8]
Au-NPs/TiO2/Au-Film (ATA)	Crystal Violet	1×10^{-7} M	[9]
Paper-based Au nanocubes	Crystal Violet	2.17×10^{-7} M	[10]
PDDA-$Ti_3C_2T_x$@AuNPs	Crystal Violet	5×10^{-11} M	This work

Table S2. The SERS detection limit of Crystal Violet compared by other's works.
The above table compares the SERS property of crystal violet under different Au composite substrate, and the result shows that PDDA-MXene@AuNPs in this work shows the most sensitive SERS property.

14. Table 3. The influence of the content of AuNPs in the PDDA-MXene@AuNPs composite for the Fenton-like process

Ration of AuNPs and PDDA-Ti$_3$C$_2$T$_x$ solution	1:10	1:5 (This work)	2:5
ICP (Au mg/L)	5.85	21.12	30.5
Degradation efficiency	79%	99%	94%

Table S3. The influence of the content of AuNPs in the PDDA-MXene@AuNPs composite for the Fenton-like process.

In the experimental section step" 4, Synthesis of PDDA- Ti3C2Tx @AuNPs composite "change the volume ratio 1:5 of AuNPs solution and PDDA-Ti$_3$C$_2$T$_x$ solution into 1:10 and 2:5. After that, investigating catalyst with different content of Au in fenton-like reactions by UV-Vis under the same conditions as that in the experimental section Step 6. The results are shown in Table S3, which demonstrate that when the content of gold is low, the catalytic efficiency decreases significantly, indicating that gold plays an important role in catalysis. However, when the gold content increases, the catalytic efficiency also decreases slightly, indicating that the increase of gold content may lead to gold agglomeration, leading to the decrease of catalytic efficiency.

References

1 B. K. Pong, H. I. Elim, J. X. Chong, W. Ji, B. L. Trout and J.Y. Lee. J. Phys. Chem. C., 2007, 111, 17, 138-139.

2 M. Shekhirev, C. E. Shuck, A. Sarycheva and Y. Gogotsi, Prog. Mater Sci., 2021, 120, 100757.

3 X. H. Pham, M. Lee, S. Shim, S. Jeong, H. M. Kim, E. Hahm, S. H. Lee, Y. S Lee, D. H. Jeong and B. H. Jun. RSC Adv., 2017, 7, 7015–7021.

4 Y. Zhang, J. Wan and Y. Ke. J. Hazard. Mater., 2010, 177, 750–754.

5 S. Liu, Y. Ying and Y. Long, Chinese. Chem. Lett., 2020, 31, 473-475.

6 M. Yu, S. Liu, D. Su, S. Jiang, G. Zhang, Y. Qin and M. Y. Li, Nanoscale., 2019, 11, 22230–22236.

7 Q. Wei, Q. Dong, D. W. Sun and H. Pu, Spectrochim. Acta A Mol. Biomol. Spectrosc., 285, 2023, 121895.

8 M. Li, J. Y. Wang, Q. Q. Chen, L. H. Lin, P. Radjenovic, H. Zhang, S. Y. Luo, Z. Q. Tian and J. F. Li. Anal. Chem., 2019, 91, 23, 15025–15031.

9 X. Zang, X. Shi, T. Oshikiri, K. Ueno, Y. Sunaba, K. Sasaki and H. Misawa, J. Phys. Chem. C., 2021, 125, 19880–19886.

10 S. Lin, X. Lin, X. Song, S. Han, L. Wang and W. Hasi. J. Raman Spectrosc, 2019, 50, 8, 1074-1084.